Chlorophyll fluorescence tracks seasonal variations of photosynthesis from leaf to canopy in a temperate forest

Running head: fluorescence and photosynthesis

Hualei Yang[1,2], Xi Yang[3,4], Yongguang Zhang[5], Mary A. Heskel[2], Xiaoliang Lu[2], J. William Munger[6], Shucun Sun[1], Jianwu Tang[2*]

[1]School of Life Sciences, Nanjing University, Jiangsu, China, 210093

[2]The Ecosystems Center, Marine Biological Laboratory, Woods Hole, Massachusetts, USA, 02543

[3]Department of Earth, Environmental and Planetary Sciences, Brown University, Providence, RI, 02912, USA

[4]Department of Environmental Sciences, University of Virginia, Charlottesville, VA, 22903, USA

[5]International Institute for Earth System Science, Nanjing University, Jiangsu, China, 210093

[6]School of Engineering and Applied Sciences and Department of Earth and Planetary Sciences, Harvard University, Cambridge, Massachusetts, USA

Corresponding author:

*Jianwu Tang, phone: 1-508-289-7162, fax: 508-457-1548, email: jtang@mbl.edu

Key words: Solar induced fluorescence; Photosynthesis; Gross primary production; Chlorophyll; Vegetation indices；Carbon cycle

Type of paper: Primary Research Article

Abstract

Accurate estimation of terrestrial gross primary productivity (GPP) remains a challenge despite its importance in the global carbon cycle. Chlorophyll fluorescence (ChlF) has been recently adopted to understand photosynthesis and its response to the environment, particularly with remote sensing data. However, it remains unclear how ChlF and photosynthesis are linked at different spatial scales across the growing season. We examined seasonal relationships between ChlF and photosynthesis at the leaf, canopy, and satellite scales, and explored how leaf-level ChlF was linked with canopy-scale solar induced chlorophyll fluorescence (SIF) in a temperate deciduous forest at Harvard Forest, Massachusetts, USA. Our results show that ChlF captured the seasonal variations of photosynthesis with significant linear relationships between ChlF and photosynthesis across the growing season over different spatial scales (R^2=0.73, 0.77 and 0.86 at leaf, canopy and ecosystem scales, respectively; $p<0.0001$). We developed a model to estimate GPP from the tower-based measurement of SIF and leaf-level ChlF parameters. The estimation of GPP from this model agreed well with flux tower observations of GPP (R^2=0.68; $p<0.0001$), demonstrating the potential of SIF for modeling GPP. At the leaf scale, we found that leaf F_q'/F_m', the fraction of absorbed photons that are used for photochemistry for a light adapted measurement from a pulse amplitude modulation fluorometer, was the best leaf fluorescence parameter to correlate with canopy-SIF yield (SIF/APAR, R^2=0.79; $p<0.0001$). We also found that canopy-SIF and SIF-derived GPP (GPP_{SIF}) were strongly correlated to leaf-level biochemistry and canopy structure, including chlorophyll content (R^2=0.65 for canopy-GPP_{SIF} and chlorophyll content; $p<0.0001$), normalized difference vegetation index (NDVI) (R^2=0.36 for canopy-GPP_{SIF} and NDVI; $p<0.0001$), and leaf area index (LAI) (R^2=0.35 for canopy-GPP_{SIF} and LAI; $p<0.0001$).

Our results suggest that ChlF can be a powerful tool to track photosynthetic rates at leaf, canopy, and ecosystem scales.

Introduction

The total production of biomass with its chemical energy converted from sunlight energy via plant photosynthesis at the canopy scale, termed gross primary productivity (GPP), drives ecosystem function and carbon cycling. At the landscape level, GPP can be estimated from eddy covariance data as the difference between net ecosystem exchange (NEE) and the total ecosystem respiration, or from remotely sensed satellite products (Heinsch *et al.*, 2006; Williams *et al.*, 2009; Zhao and Running, 2010; Frankenberg et al., 2011; Jung *et al.*, 2011; Migliavacca *et al.*, 2011; Miura *et al.*, 2000). However, direct measurement of GPP at the landscape or regional scale is not available. The Monteith (1972; 1977) model has been used to calculate GPP as a function of absorbed light energy (i.e. absorbed photosynthetically active radiation, APAR) multiplied by the light use efficiency (ε) that converts light energy to chemical energy stored as plant biomass (i.e. GPP=APAR*ε). Unfortunately, it is challenging to accurately estimate light use efficiency (ε) and APAR at large scales because these parameters may vary with different biomes, physiological factors, and environmental conditions (Medlyn, 1998; Frankenberg *et al.*, 2011). Therefore, there is a critical need to develop a more accurate method to estimate GPP and its temporal variation through seasons.

Light energy captured by the leaf chlorophyll molecules and transferred to the reaction centers is released via three different pathways, photochemistry, non-photochemical quenching (NPQ, i.e. heat dissipation), and a small fraction re-emitted as chlorophyll fluorescence (ChlF). More recently, advancements in measurement techniques have found that ChlF detected at the

canopy and landscape scales correlated with photosynthesis and/or GPP at those scales (Guanter *et al.*, 2012; Guanter *et al.*, 2014; Lee *et al.*, 2013; Yang *et al.*, 2015).

Using fluorescence signals to derive leaf photosynthesis or canopy GPP at multiple scales has received increasing attention. At the leaf scale, many pulse amplitude modulation (PAM) fluorometers have been developed to simultaneously measure ChlF and photosynthetic CO_2 uptake (Bolhar-Nordenkampf *et al.*, 1989; Rascher *et al.*, 2000; Naumann *et al.*, 2007; Galle *et al.*, 2009; Van der Tol *et al.*, 2014). The PAM fluorometers, which integrate a gas-exchange system with a fluorescence chamber head, can accurately measure plant photosynthetic physiology *in vivo* (Long and Bernacchi, 2003). At the larger scale, using solar induced chlorophyll fluorescence (SIF) signals over a narrow spectral region on remote sensing platforms (e.g. above-canopy towers, aircrafts, and satellites) has grown over the past decade in order to estimate GPP (Grace *et al.*, 2007; Baker, 2008; Meroni *et al.*, 2009; Rascher *et al.*, 2009; Damm *et al.*, 2010; Frankenberg *et al.*, 2011; Joiner *et al.*, 2011; Joiner *et al.*, 2012; Joiner *et al.*, 2013; Porcar-Castell *et al.*, 2014). Currently, spectroradiometer systems that observe tower (canopy)-SIF signal based on the measurements of solar irradiance and vegetation radiance have recorded a strong relationship between SIF and GPP at the canopy scale (Rossini *et al.*, 2010; Yang *et al.*, 2015). At the global scale, satellite technologies have been developed to retrieve the regional SIF signal, e.g. the Greenhouse Gases Observing Satellite (GOSAT) and Global Ozone Monitoring Experiment 2 (GOME-2) (Joiner *et al.*, 2011; Frankenberg *et al.*, 2011; Guanter et al. 2012; Joiner *et al.*, 2013). Joiner et al. (2013) demonstrated that the spatial and temporal variability in SIF derived from GOME-2 agreed with that of GOSAT-SIF. Satellite observation of terrestrial chlorophyll fluorescence could provide important information on plant growth status, the carbon balance of terrestrial ecosystems, and the length of the carbon uptake period (Guanter

et al. 2014; Zhang *et al*., 2014; Lee *et al*. 2015). However, at present, little is known about the linkage between leaf-level ChlF and canopy-SIF.

In addition, the relationship between SIF and GPP is not fully understood. Some researchers reported that SIF exhibited a strong linear correlation with GPP on the global (Frankenberg *et al*., 2011; Guanter *et al*., 2012) and canopy level (Guanter *et al*. 2013; Yang *et al*., 2015). Others considered the relationship between SIF and GPP could not be strictly linear and the application of a linear relationship between SIF and GPP could introduce biases in the estimation of GPP (e.g. Lee *et al*. 2015).

In this study, we measure chlorophyll fluorescence and carbon exchange at both leaf and canopy scales at Harvard Forest, MA, USA, with the objective of more accurately characterizing the relationship between SIF and GPP. Our primary goals are (1) to investigate the seasonal dynamics of ChlF and photosynthesis and study their correlations at different spatial scales during the growing season; (2) to explore the linkages between leaf-level ChlF parameters and the canopy- and satellite-level SIF; and (3) to predict GPP from SIF measurements and compare the SIF-derived GPP with eddy covariance-based GPP.

Materials and methods

Site description

Chlorophyll fluorescence and gas exchange measurements on the leaf scale were conducted on a walk-up tower site, which is located at a hardwood stand at the Harvard Forest, Petersham, Massachusetts, USA (42°32′6″ N, 72°10′28″ W). The site is characterized with cool, moist temperate climate with average temperatures of -7°C in January and 20°C in July. The annual precipitation is averaged at 1,100 mm, distributed evenly throughout the year. Snow

typically covers the ground for several months during winter. The approximately 80-100 years old mixed hardwood stand is dominated by red oak (*Quercus rubra.*), red maple (*Acer rubrum L.*), and American beech (*Fagus grandifolia Ehrh.*). Soils are mainly sandy loam glacial till, with some alluvial and colluvial deposits. Photosynthetically active radiation (PAR) and air temperature data were collected from the walk-up tower. The canopy-level SIF data were collected from the nearby barn tower (Yang *et al.*, 2015). An eddy covariance tower at the Environmental Monitoring site (EMS) measured CO_2 exchange and environmental data. These three locations are within 1.5 kilometer from each other and covered by similar vegetation composition and soil types.

Chlorophyll fluorescence

We used a LI-6400XT with an integrated leaf chamber fluorometer (LCF) (LI-6400-40; LI-COR, Inc., Lincoln, NE, USA), a pulse amplitude modulation (PAM) system that has an LED-based fluorescence source accessory to simultaneously measure leaf-based chlorophyll fluorescence and photosynthesis rates. The rapid and non-destructive measurements of leaf chlorophyll fluorescence were conducted on randomly selected leaves from *Fagus grandifolia Ehrh.* and *Quercus rubra.* trees. We selected 3-5 leaves from each canopy heights (2, 7, 12, 17 and 23 m) at different time of the day (n = 90 per day) (daily in spring and autumn and monthly in summer) and used LI-6400XT in *situ.* We used light of different intensities on a dark-adapted and a light adapted leaf to estimate fluorescence kinetics (i.e. the Kautsky curve) (Bradbury and Baker, 1981; Baker, 2008). When a leaf was placed in the dark for more than 30 minutes (Larcher and Cernusca, 1985), the PSII reaction centers were completely open (i.e. the

primary quinone electron acceptor (QA) was oxidized). Then the dark-adapted leaf was exposed to a weak red light (intensity was 3 μmol $m^{-2}s^{-1}$) with wavelength centered at 630 nm and the LCF detected the initial minimum fluorescence, termed F_o. Then after the leaf was exposed to saturated flash lights (light intensity> 7,000 μmol $m^{-2}s^{-1}$), there was an immediate rise in fluorescence to an initial maximal level, termed F_m, representing that the PSII reaction centers were completely closed and fluorescence maximized. Another leaf was measured for the light adapted process. With an actinic light provided by LCF at the intensity that was adjusted equivalent to the ambient light to drive photosynthesis, the fluorescence reached a stable state on 715nm wavelength, termed F_s. The actinic light was turned off, and a weak far red light (the wavelength centered at about 740 nm with the intensity of 30 μmol $m^{-2}s^{-1}$) was emitted to measure minimal fluorescence of the light adapted leaf, termed F_o'. The fluorescence rose to a maximum when the light-adapted leaf was exposed to a brief saturating flash (similar to that of the dark-adapted leaf), termed F_m'. Normally, F_o' is higher than F_o and F_m' is lower than F_m, since the reaction centers cannot completely open for F_o' or completely close for F_m' for the light-adapted leaf. Thus, the fluorescence parameters can be calculated by the following formulas:

$$F_v/F_m = \frac{F_m - F_o}{F_m} \qquad (1)$$

where F_v/F_m means the fraction of absorbed photons that are used for photochemistry for a dark adapted leaf, which usually reflects the potential photosynthetic capacity or photosynthetic efficiency of plants. F_o and F_m are the dark-adapted minimum and maximum fluorescence, respectively.

$$F_q'/F_m' = \frac{F_m' - F_s}{F_m'} \qquad (2)$$

where F_q'/F_m' is the fraction of absorbed photons that are used for photochemistry for a light adapted leaf (photochemical yield). F_s is the steady-state fluorescence, and F_m' is the maximal value under a saturating flash light. All the leaf-scale fluorescence parameters were averaged across leaves from different species and canopy locations as the daily mean values.

For the canopy fluorescence signal observation, we used a recently published technique (Yang *et al.*, 2015) to continuously (at 5-minute intervals) measure solar-induced fluorescence (SIF) from a spectrometric system from May to October, 2014. The spectrometer, capable of measuring spectra with a spectral resolution of ~0.13 nm between 680 nm and 760 nm (HR2000+, OceanOptics, Inc., Dunedin, FL.), was connected to two fiber optic cables, one of which was pointed vertically towards the sky collecting total solar irradiance, and the other towards the target canopy (viewing zenith angle: 30°) measuring the vegetation radiance. The paired solar irradiance and vegetation radiance were recorded every 5 minutes and converted to valid data with the units of $mWm^{-2}nm^{-1}$ and $mWm^{-2}sr^{-1}nm^{-1}$ for irradiance and radiance, respectively, with radiometric calibration. Finally, we calculated the SIF at 760 nm from the irradiance and radiance observations under clear sky conditions (When diffuse radiation/ (diffuse radiation + direct radiation) <0.5) by using the spectral fitting methods (SFM) (Meroni *et al.*, 2009; Yang *et al.* 2015). Daily mean SIF between 6:00 AM and 6:00 PM was calculated, and the outliers (due to overcast or machine error) were removed from subsequent graphs for clarity.

We used data from satellite GOME-2 (The Global Ozone Monitoring Experiment-2) level 2 products that provided SIF referenced to 740nm (SIF_{740}) with ~0.5nm spectral resolution (spatial resolution is 40km×80 km) (Joiner *et al.*, 2013). Monthly SIF_{740} was extracted at the pixel covering Harvard Forest from May to October in 2014. To compare with the canopy SIF_{760}, GOME-2 SIF_{740} was converted to SIF_{760} by multiplying by a specific coefficient 0.582 (Yang *et*

177 *al.*, 2015). The monthly GOME-2 SIF_{760} time series data were smoothed using the
178 Savitzky-Golay filter.
179
180 **Gas exchange measurements**
181 Leaf net photosynthetic rate (P_{net}, μmol $m^{-2}s^{-1}$) was quantified in parallel with the
182 measurements of leaf fluorescence using an open gas exchange system (LI-6400XT; LI-COR,
183 Inc., USA) under a imposed light intensity (i.e. PAR) according to the ambient radiance with a
184 constant CO_2 level around 400 μmol $m^{-2}s^{-1}$, and during the plant growing season (Xu *et al.*, 2008).
185 We calculated leaf apparent photosynthesis ($P_{apparent}$) as dark respiration (P_{net} when PAR = 0)
186 plus P_{net} at a given light intensity (Wohlfahrt and Gu, 2015). Our measurements did not include
187 simultaneous estimates of photorespiration, thus limiting our ability to calculate true gross
188 photosynthesis (Wohlfahrt and Gu, 2015). Daily mean $P_{apparent}$ was calculated as the average of
189 the values across the leaves from different canopy layers over the course of a day. In addition, we
190 measured light response curves of $P_{apparent}$ and F_q'/F_m'. The leaf was illuminated for 20-30 min
191 until steady-state fluorescence and gas exchange values were recorded. The irradiances used for
192 the light response curve were 50, 100, 300, 500, 800, 1200 and 1600 μmol $m^{-2}s^{-1}$.
193 Daily mean GPP at the canopy scale was calculated from data collected using the eddy
194 covariance techniques. We applied REddyProcWeb online tool
195 (http://www.bgc-jena.mpg.de/bgi/index.php/Services/REddyProcWeb) with the eddy covariance
196 and meteorological data on EMS (Environmental Monitoring Station) tower at Harvard Forest,
197 and used the flux partitioning algorithms to partition net ecosystem (NEE) into GPP and
198 ecosystem respiration (Reichstein *et al.*, 2005; Yang *et al.*, 2015). Daily mean GPP (GPP_{EC}) was
199 calculated as the ratio of the sum of hourly GPP to the daytime length (PAR>0 μmol $m^{-2}s^{-1}$). Also,
200 for the satellite-based GPP (GPP_{SAT}), 8-day 1km Moderate Resolution Imaging

Spectroradiometer (MODIS) GPP (MOD17A2) data of Harvard Forest (within approximately the same tower averaging area) in year 2014 were downloaded (http://modis-land.gsfc.nasa.gov/).

Leaf traits and vegetation indices

We used a Soil Plant Analysis Development (SPAD)-502 meter (Spectrum Technologies, Aurora, IL, USA) to monitor changes of chlorophyll concentration during the growing season. This non-destructive technique has been used to estimate leaf chlorophyll concentration rapidly and accurately by measuring the leaf transmittance in two wavebands centered at 650 nm and 940 nm. We selected 15 sun-lit leaves from the top of the canopy of the *Quercus rubra* and *Fagus grandifolia Ehrh.* each day, and made five SPAD readings for each leaf that were evenly distributed over the whole leaf area. We found that there was no difference in SPAD values between *Quercus rubra* and *Fagus grandifolia Ehrh.* by t-tests in Excel with species as a factor ($t=0.47$; $p=0.64$); hence, average SPAD across leaves and the two species were made per day to calculate SPAD of the stand.

To estimate seasonality of vegetation development from spring leaf-out to autumn senescence, we used a tower-based Tetracam Agriculture Digital Camera (Tetracam, Inc., Chatsworth, CA.) during the growing season as a simple and accurate technique to monitor vegetation reflectance in visible and near-infrared bands to estimate canopy Normalized Difference Vegetation Index (NDVI). Leaf area index (LAI) of the forest was measured using a LAI-2000 Plant Canopy Analyzer (LI-COR, Inc., Lincoln, NE, USA), when the sun was near the horizon (before sunrise or after sunset), or on overcast days to reduce the contribution of scattered radiation.

To investigate the independent effects of vegetation structure (LAI) and leaf physiology (chlorophyll) on SIF variability, a one-by-one sensitivity analysis was performed with the SCOPE model (Soil Canopy Observation of Photosynthesis and the Energy Balance) (Van der tol *et al*, 2009b) with the most informative leaf optical properties and canopy structural variables: maximum carboxylation capacity (Vcmo), leaf chlorophyll content (Cab), leaf inclination (LIDFa), incoming shortwave radiation (Rin), and leaf area index (LAI) (Zhang *et al.*, 2016).

Estimation of GPP using SIF

We calculated canopy GPP using measurements of SIF and extended the relationship between photosynthesis and fluorescence from the leaf scale to the canopy. Since chlorophyll fluorescence (ChlF), here measured as canopy-scale SIF and leaf-scale F_s, is a byproduct of the light-reactions of photosynthesis, we can evaluate ChlF as the product of absorbed radiation and light use efficiency (Guanter *et al*. 2014) in a similar way to photosynthesis expressed as light intensity and photosynthesis efficiency, i.e., photosynthesis or fluorescence can be calculated as the product of absorbed light intensity and photosynthesis quantum efficiency (ε_P) or fluorescence quantum efficiency (ε_F) (Lee *et al*. 2015):

At the leaf scale:

$$P_{\text{apparent}} = \text{APAR}_L * \varepsilon_{PL} \quad (3)$$

$$F_s = \text{APAR}_L * \varepsilon_{FL} \quad (4)$$

At the canopy scale:

$$\text{GPP} = \text{APAR}_C * \varepsilon_{PC} \quad (5)$$

$$\text{SIF} = \text{APAR}_C * \varepsilon_{FC} \quad (6)$$

where ε_{PL} and ε_{FL} are photosynthesis quantum efficiency and fluorescence quantum efficiency, respectively, at the leaf scale, and ε_{PC} and ε_{FC} are photosynthesis quantum efficiency and fluorescence quantum efficiency, respectively, at the canopy scale. $APAR_L$ is the absorbed photosynthetically active radiation ($\mu mol/m^2/s$) at the leaf scale, and can be calculated as $APAR_L = PAR * f * \alpha_{leaf}$. PAR refers to the imposed photosynthetically active radiation ($\mu mol\ m^{-2}s^{-1}$) from LiCor 6400-LCF, f is the fraction of absorbed photos that are used by PS II (usually is 0.5 for C3 plants), and α_{leaf} means leaf absorptivity and is typically estimated to 0.84 (Genty *et al.*, 1989). $APAR_C$ is the absorbed photosynthetically active radiation ($\mu mol/m^2/s$) at the canopy scale and can be calculated as $APAR_c=PAR_{up}-PAR_{reflect}-PAR_{under}$ (Yang *et al.*, 2015). PAR_{up}, $PAR_{reflect}$ and PAR_{under} are solar incident PAR, reflected PAR from canopy, and lower-canopy incident PAR, respectively.

Both F_s and SIF refer to the light-adapted steady-state fluorescence value. Measured F_s is a relative, unitless value and cannot be directly compared to SIF. So we provide a correction coefficient (c) to represent actual F_s (i.e. $c*F_s$ for corrected F_s). Here, c is an instrument-specific constant, calculated as below (Eq. 9).

The PAR conversion efficiency (ε) can be parameterized as a function of meteorological parameters and varies with different vegetation types (Field *et al.*, 1995; Prince and Goward 1995; Turner *et al.* 2003). We assumed the value of leaf scale ε_{PL} or ε_{FL} across leaves from different canopy layers represents the canopy-scale ε_{PC} or ε_{FC} (Middleton *et al.*, 2009), i.e., $\varepsilon_{PL} = \varepsilon_{PC}$, $\varepsilon_{FL} = \varepsilon_{FC}$. Therefore,

$$\frac{P_{\text{apparent}}}{\text{APAR}_\text{L}} = \frac{\text{GPP}}{\text{APAR}_\text{C}} \qquad (7)$$

$$\frac{\text{c} * F_\text{s}}{\text{APAR}_\text{L}} = \frac{\text{SIF}}{\text{APAR}_\text{C}} \qquad (8)$$

Under a given incident light (for example, PAR=600μmol $m^{-2}s^{-1}$) on leaf and canopy scales, the correction coefficient (*c*) can be calculated from equation (9):

$$c = \frac{\mathrm{APAR_L}}{\mathrm{APAR_C}} * \frac{\mathrm{SIF}}{F_s} \qquad (9)$$

Using the measured values during the growing season, *c* values were found to be relatively stable around 0.0001, therefore, *c* value was typically assumed as 0.0001(mW/m^2/sr/nm per F_s count) in this study.

From equation (7) and (8), we derive a relationship between GPP and SIF:

$$\mathrm{GPP} = (P_{\mathrm{apparent}} / (c * F_s)) * \mathrm{SIF} \qquad (10), \text{ or}$$

$$\mathrm{GPP/SIF} = P_{\mathrm{apparent}}/(c*F_s) \qquad (11)$$

Eqs. 10 and 11 show that GPP at the canopy scale can be calculated from SIF measurements, given the known leaf-scale parameter, $P_{\mathrm{apparent}}/(c*F_s)$. Thus, estimated GPP from SIF can be independently compared with the eddy covariance-based GPP and satellite-based GPP.

Results

The seasonality of leaf chlorophyll fluorescence and photosynthesis parameters over different spatial scales

Seasonal patterns of leaf chlorophyll fluorescence and photosynthesis were observed at the leaf, canopy, and satellite levels (Fig. 1). According to the previous study on the seasonality of the vegetation indices and plant physiological traits based on the NDVI (Normalized Difference Vegetation Index) measured by an NDVI camera and leaf chlorophyll concentration

285 at this site, we identified spring (DOY 132-167), summer (DOY 168-260) and autumn (DOY

286 261-311) (Yang *et al*., 2016; Yang *et al*., 2016).

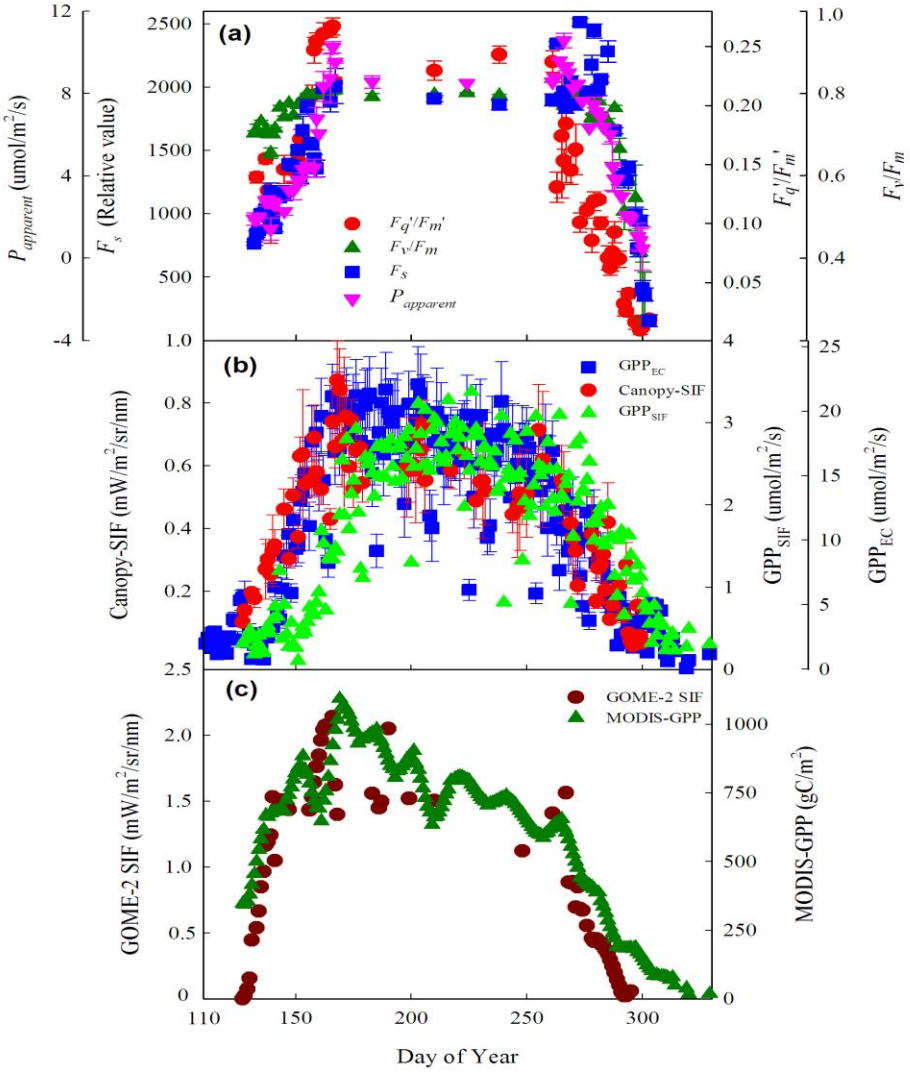

287

288 Fig. 1 The seasonality of leaf chlorophyll fluorescence and photosynthesis over different spatial scales. (a)

289 leaf-scaled chlorophyll fluorescence parameters: steady-state fluorescence (F_s), photochemistry efficiency

290 of dark-adapted leaf (F_v/F_m), photochemistry efficiency of light-adapted leaf (F_q'/F_m'), leaf apparent

291 photosynthesis ($P_{apparent}$); (b) canopy-scaled solor-induced fluorescence (SIF) and it derived gross primary

292 productivity (GPP_{SIF}), and eddy covariance tower-based GPP (GPP_{EC}); (c) smoothed GOME-2 SIF and

293 MODIS-GPP. The error bars are ± 1SE.

On the leaf scale, the ChlF parameters (F_s, F_v/F_m, F_q'/F_m') and photosynthetic rate ($P_{apparent}$) increased after leaf emergence and reached to summer peak around DOY 168 (for example, F_s and $P_{apparent}$ increased 70%). In autumn, F_q'/F_m' and $P_{apparent}$ decreased from late-September (DOY 261) due to the leaf aging, and the decline appeared earlier (~10 days) than other leaf ChlF parameters (F_s, F_v/F_m). On the canopy scale, similar seasonality trajectories appeared among SIF, GPP_{SIF} and GPP_{EC} over the growing season. In the seasonal cycle, onset of canopy-SIF and its derived GPP (GPP_{SIF}) appeared on DOY 127, a week earlier compared to GPP_{EC} (eddy flux GPP) after leaf emergence at the beginning of May. SIF, GPP_{SIF} and GPP_{EC} had a rapid increase with green-up in spring until late June (approximately DOY 167) and reached its maximum around the middle summer, then sharply decreased from mid-September (~DOY 260) in the autumn due to leaf senescence and aging until dormancy period. For the satellite fluorescence and photosynthesis data, smoothed GOME-2 SIF and MODIS-GPP showed more fluctuation than SIF and GPP measured at the canopy scale, because of its coarse spatial and temporal resolution. Both GOME-2 SIF and MODIS-GPP increased in the spring season and reached the summer peak on DOY 167, and then declined slightly during the late summer season and rapidly in autumn starting DOY 265.

In general, the seasonal changes of ChlF appeared roughly synchronous with that of photosynthesis in leaf, canopy and satellite scales. Furthermore, the spring rising points and autumn decline points of ChlF and photosynthesis parameters appeared earlier on the canopy and satellite scale than leaf level. ChlF and photosynthesis at all scales reached summer peak around DOY 167. Overall, the ChlF values were higher in spring than that in fall.

Leaf fluorescence parameters correlated with canopy SIF and GOME-2 SIF (Fig. 2). Strong correlations existed between F_q'/F_m' (indicating quantum yield of PS II at the leaf scale

under a light condition) and canopy SIF (spring R^2 =0.64, fall R^2=0.75), and between F_q'/F_m' and GOME-2 SIF (spring R^2 = 0.64, fall R^2=0.77), with all regressions highly significant ($p<0.0001$). We also found that leaf-level ChlF and canopy SIF (or GOME-2 SIF) showed different slopes for spring and fall.

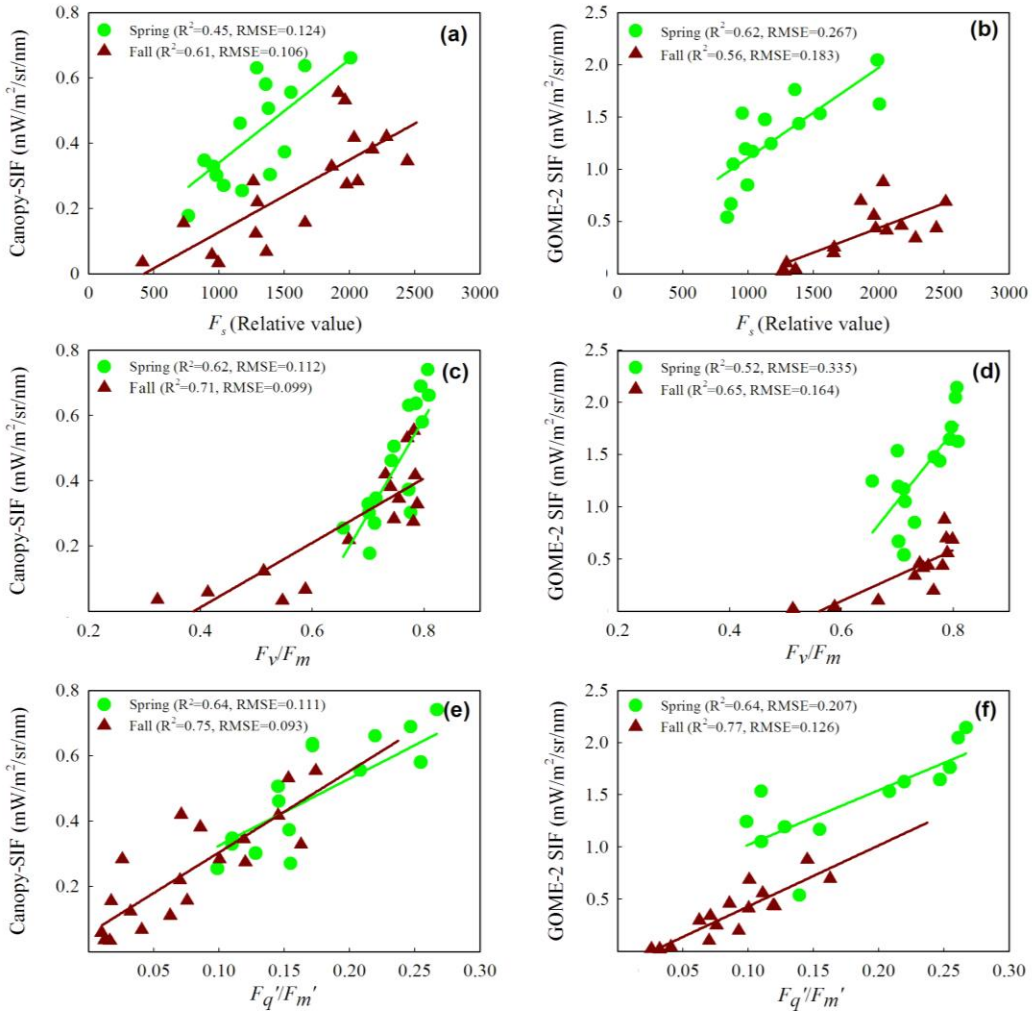

Fig. 2 The seasonal relationships between daily mean leaf-scaled fluorescence parameters and up-scaled SIF. (a)(b) linear relationships between leaf-scaled steady-state fluorescence (F_s) and canopy-SIF and GOME-2 SIF, respectively; (c)(d) linear relationships between leaf-scaled F_v/F_m and canopy-SIF and

GOME-2 SIF, respectively; (e)(f) linear relationships between leaf-scaled F_q'/F_m' and canopy-SIF and GOME-2 SIF, respectively.

We examined the correlations between F_q'/F_m' (photochemical yield) and canopy-SIF/APAR (SIF yield), and found that the SIF yield was linearly increasing with photochemical yield under high light conditions (Fig. 3), which is generally the overpass time of satellite observations of SIF.

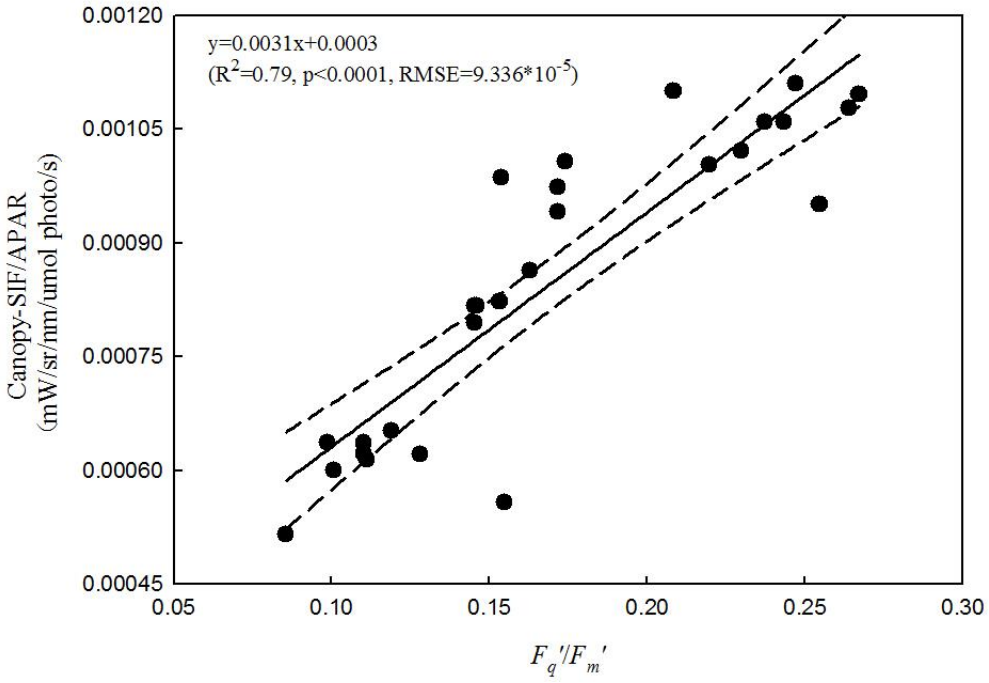

Fig. 3 The correlation between photochemical yield (*Fq'/Fm'*) and SIF yield (canopy-SIF/APAR) under 500-1000 μmol $m^{-2}s^{-1}$ light intensity. The dotted lines represent 95% confidence interval. Coupled *Fq'/Fm'* and canopy-SIF/APAR were selected under the same light condition.

Correlations between plant chlorophyll fluorescence and photosynthesis

There were significant seasonal relationships between ChlF and photosynthesis from leaf to satellite scales, explained by the gradual spring increases and autumn decreases in deciduous forest. At the leaf scale, the fluorescence parameter F_q'/F_m' was strongly linked to $P_{apparent}$ (R^2=0.76, 0.82 and 0.49 for spring, fall and entire growing season, respectively; p<0.0001), and F_s was highly related to $P_{apparent}$ (R^2=0.70, 0.82 and 0.73 for spring, fall and entire growing season, respectively; p<0.0001) (Fig. 4a, 4b). F_q'/F_m' had a declining light response curve, in contrast to that of $P_{apparent}$ (Fig. 5). Photosynthesis is a photobiochemical reaction process, and $P_{apparent}$ will accelerate rapidly with an increase of light intensity, but beyond a certain range (800-1200 μmol $m^{-2}s^{-1}$), $P_{apparent}$ increases slowly until it is saturated. On the contrary, with the increasing light intensity, F_q'/F_m' declined gradually and became saturation approximately under 1000 μmol $m^{-2}s^{-1}$ light condition (Fig. 5).

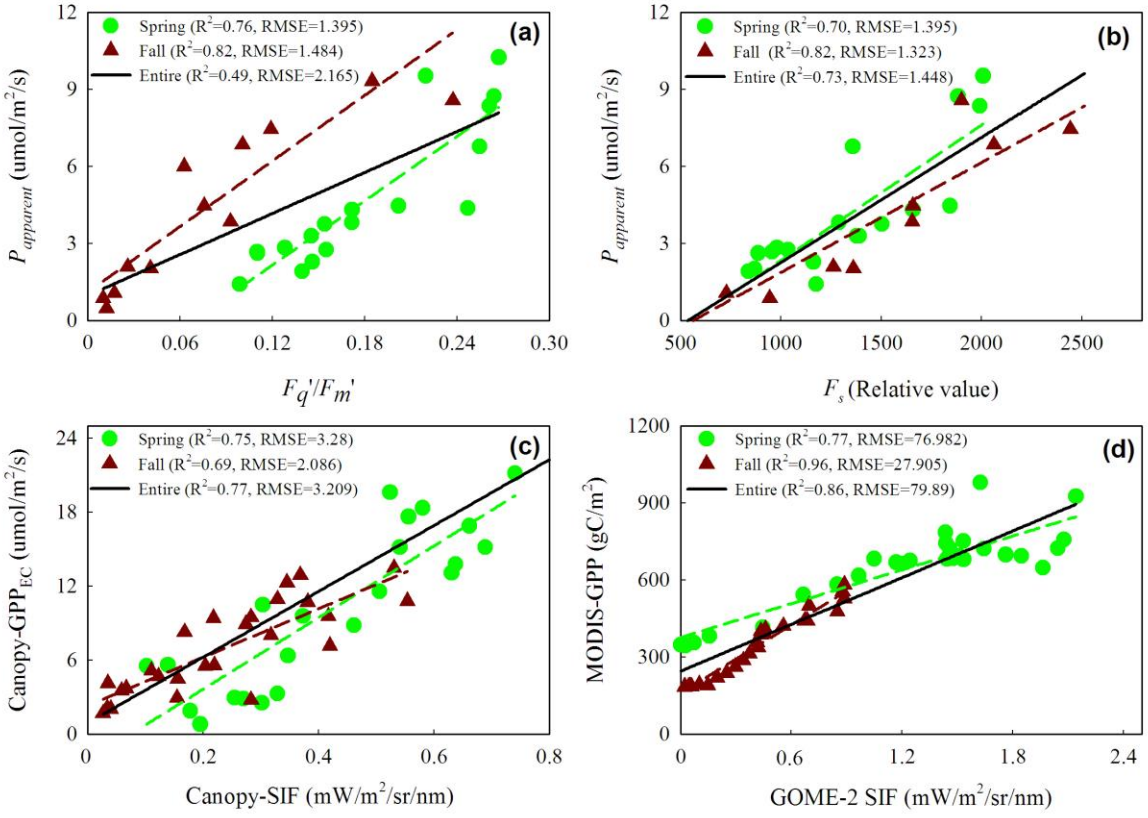

Fig. 4 The correlations between daily mean chlorophyll fluorescence and photosynthesis over different spatial scales. (a) linear regressions between photochemesitry efficient (F_q'/F_m') and apparent photosynthetic rate ($P_{apparent}$); (b) linear regressions between steady-state fluorescence (F_s) and $P_{apparent}$; (c) linear regressions between canopy-SIF and eddy covariance GPP; (d) linear regressions between GOME-2 SIF and MODIS-GPP.

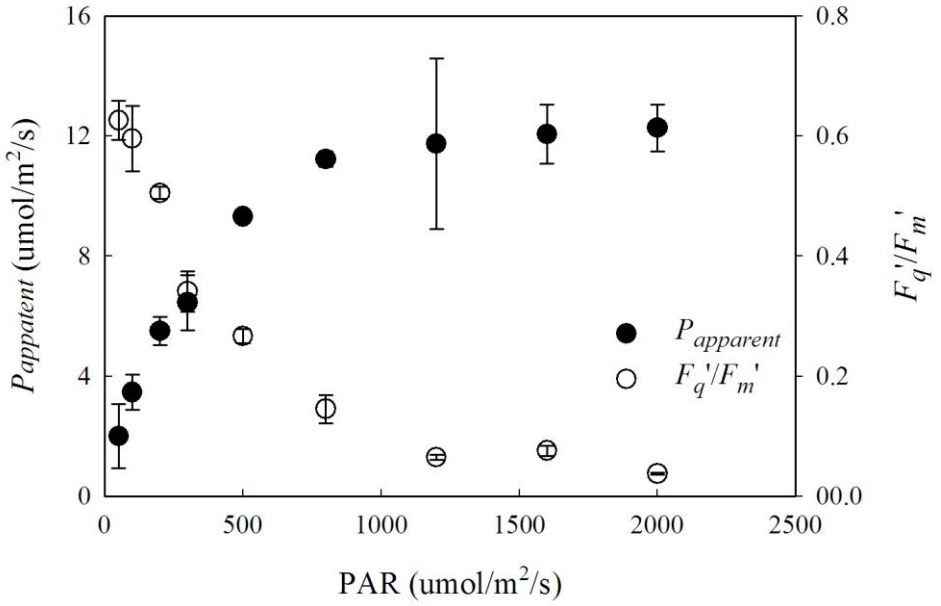

Fig. 5 The light response curves of F_q'/F_m' and $P_{apparent}$. The error bars are ± 1SE.

At the canopy scale, SIF demonstrated a similar seasonal trend to GPP. Canopy-level SIF was positively correlated with GPP_{EC} (R^2=0.75 0.69 and 0.77 in spring, fall and, entire growing season, respectively; p<0.0001) (Fig. 4c). Similarly on satellite scales, GOME-2 SIF was positively related to MODIS-GPP with the high correlation coefficients (R^2=0.77, 0.96 and 0.86 in spring, fall and entire growing season, respectively; p<0.0001) (Fig. 4d).

Estimating GPP using SIF based on leaf-scaled physiological properties

After comparing SIF-derived GPP (GPP_{SIF}) and eddy covariance tower-based GPP (GPP_{EC}) at the canopy scale, we found that GPP_{SIF} and GPP_{EC} had similar seasonal dynamics during the growing season that could be associated with phenological process in the deciduous forest (Fig. 1). The one-to-one regression results indicated that GPP_{SIF} was 1.065 times of GPP_{EC} (R^2=0.68; p<0.0001; RMSE=4.0) (Fig. 6).

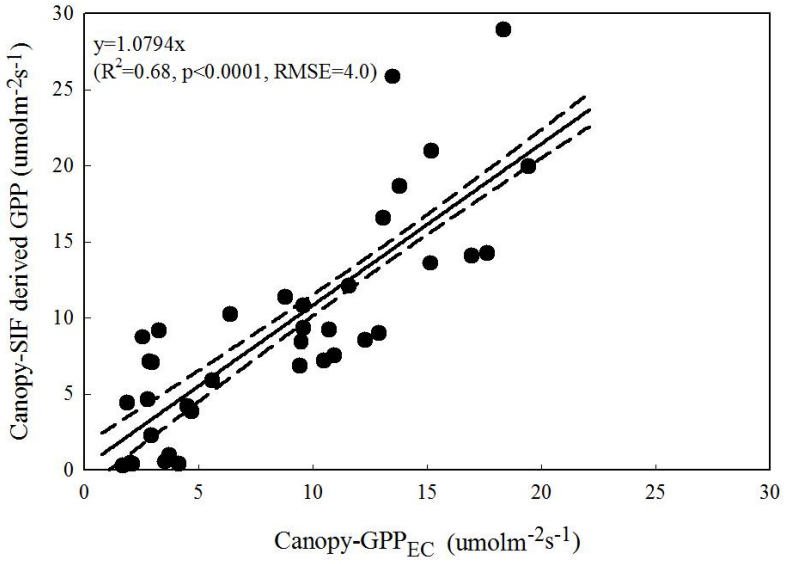

Fig. 6 The linear correlation between canopy GPP_{EC} and SIF-derived GPP (GPP_{SIF}) over 2014 growing season. The dotted lines represent 95% confidence interval.

SIF-derived GPP correlated with chlorophyll content and vegetation indices

Remotely sensed SIF as well as SIF-derived GPP can reflect vegetation phenological pattern and relate to the biochemical (chlorophyll content) and structural (NDVI and LAI) parameters of the plants. Our results showed that SIF-derived GPP highly related with leaf chlorophyll content (R^2=0.65; p<0.0001) (Fig. 7a). Concerning the relationships between GPP_{SIF} and other vegetation indices that are typically linked to seasonal morphological development of plant canopies, both LAI and NDVI were significantly related to the seasonal dynamics of

381 GPP_{SIF} (R^2=0.35 between GPP_{SIF} and LAI; R^2=0.36 between GPP_{SIF} and NDVI; p<0.0001) (Fig.

382 7b and Fig. 7c).

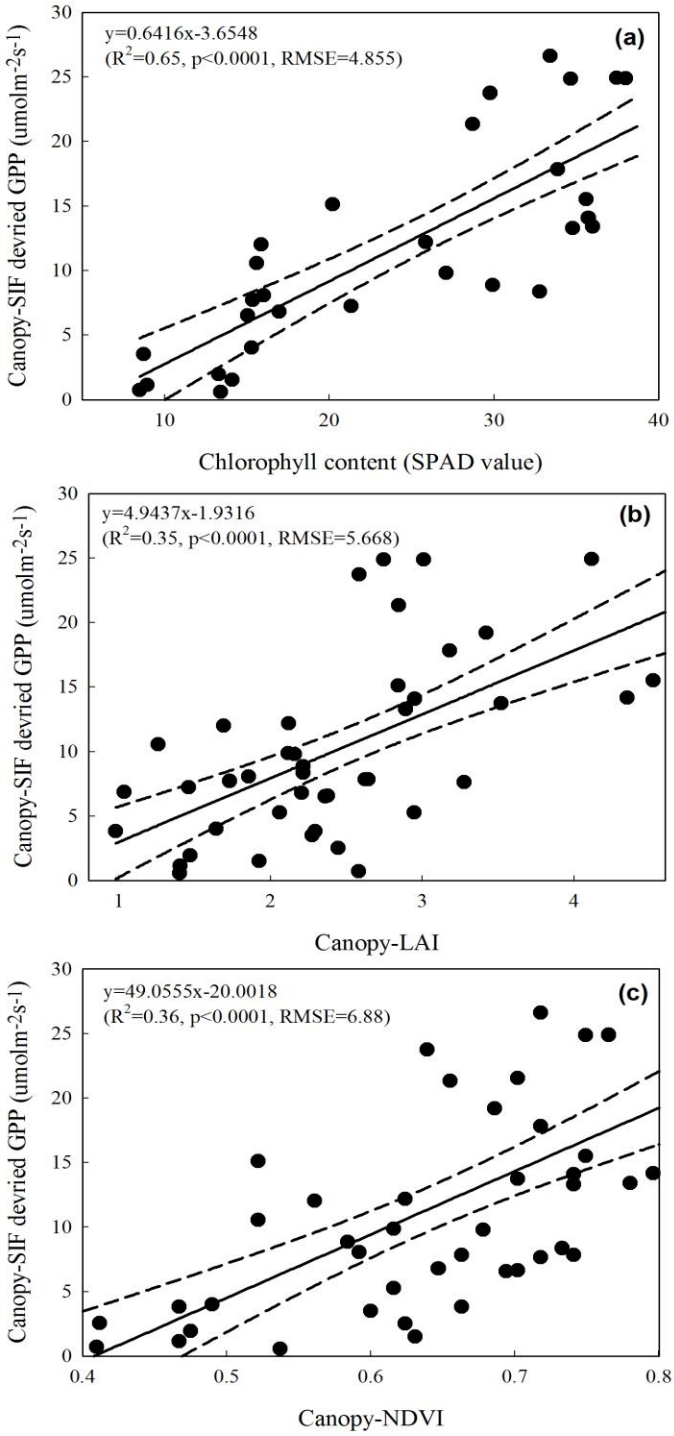

383

Fig. 7 SIF-derived GPP_{SIF} was significantly related to plant physiological and functional characteristics. The dotted lines represent 95% confidence interval.

Fig. 8 shows the independent influence of LAI and leaf chlorophyll content (Cab) on SIF variability. On the one hand, when LAI was fixed, SCOPE-SIF_{760} increased with increased Cab and reached saturation at the point that Cab was around 25 μg/cm^2 (Fig. 8a). On the other hand, SCOPE-SIF_{760} increased with increasing canopy-LAI, and the rising curves between SCOPE-SIF_{760} and LAI under Cab=40 and Cab=60 were very close with each other (Fig. 8b).

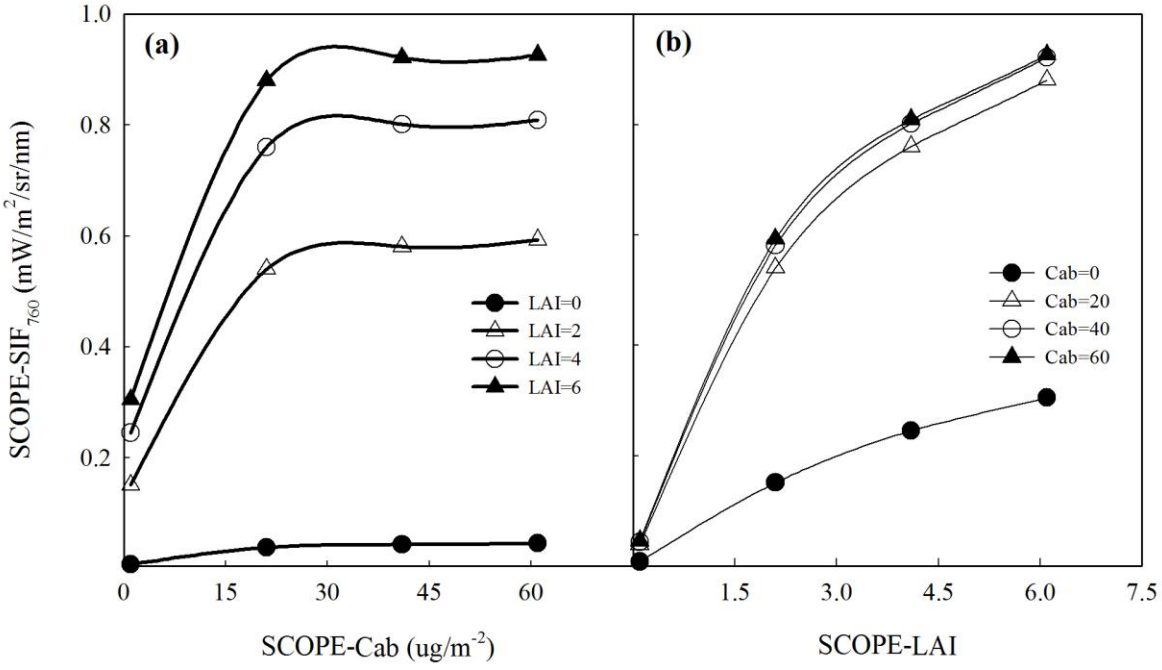

Fig. 8 The independent influence of leaf chlorophyll content (Cab) and LAI on SIF variability by fixing the maximum carboxylation capacity (Vcmo), incoming shortwave radiation (Rin), leaf inclination (LIDFa) as 100 μmol m^{-2} s^{-1}, 800Wm^{-2}, -1, respectively. All the values are simulated by SCOPE model.

Discussion

In this study, we investigated the relationships between leaf-level ChlF parameters and canopy- or satellite-SIF, and the correlations between ChlF and plant photosynthetic capacity over multiple spatial scales.

The linkages between leaf and canopy fluorescence

We measured ChlF parameters from leaf to canopy and satellite scales. At the leaf level, the F_v/F_m represents the maximal quantum yield used for photochemistry (Kitajima and Butler, 1975). All green leaves that we measured were typically in the range of 0.75-0.85, consistent with previous results (Flexas *et al*., 2002). In unstressed environmental conditions, with increasing light intensity, the fraction of light energy used for photochemistry decreases and the fraction of light energy used for fluorescence increases (Seaton and Walker, 1990; Maxwell and Johnson, 2000;Van der Tol *et al*., 2009a). F_q'/F_m' decreased in high light conditions because of increases in non-photochemical quenching (NPQ, i.e. heat dissipation), that reflecting a plant protection mechanism to avoid over-energization of the thylakoid membranes (Baker, 2008).

F_v/F_m and F_q'/F_m' are sensitive to physiological and environmental changes that affect the ability to capture light energy by open PSII reaction centers. F_q'/F_m' and CO_2 fixation capacity ($P_{apparent}$) showed greater difference in slopes for the spring and fall correlations than that between F_s and $P_{apparent}$ (Fig. 4a, 4b). With increased light intensity, the carbon fixation rate gradually increased and became light saturated, along with a decrease in photochemistry yield (i.e. F_q'/F_m') (Fig. 5) (Porcor-Castell *et al.*, 2014).

Leaf-scale ChlF parameters showed seasonally-dependent correlations with SIF (canopy-SIF and GOME-2 SIF), and the slopes of the linear regressions were different for spring and autumn. F_v/F_m, which means maximum photosynthetic capacity, is usually stable for a

421 healthy leaf; so the decline of F_v/F_m and the concurrently decline of canopy SIF (Fig. 2c) may
422 directly prove that SIF could track photosynthetic capacity.

423 Also, we found that F_q'/F_m' showed better agreement with canopy-scale SIF than other
424 leaf-scaled fluorescence parameters (F_s, F_v/F_m) (Fig. 2), indicating that F_q'/F_m', which involved
425 leaf steady fluorescence (F_s) and actual maximal fluorescence (F_m'), was the best leaf-scale
426 fluorescence parameter to interpret the up-scaled fluorescence level. This consistency between
427 F_q'/F_m' and canopy-SIF may be due to both of them indicating the information of electron
428 transport rate (ETR) (Baker, 2008); in other words, canopy-SIF could capture leaf-level
429 variations of ETR. This also supported the simulations by Guan *et al*. (2016) in which they
430 showed the linear relationship between ETR and SIF for several crops. Furthermore, there was a
431 significant, positive relationship between photochemical yield (F_q'/F_m') and SIF yield
432 (canopy-SIF/APAR) under high light conditions (Fig. 3), since both of photochemical yield and
433 SIF yield decreased with increasing NPQ (Lee *et al*., 2015). This finding from the field
434 measurement supports the previous modeling result at canopy level (Lee *et al*., 2015; Guan *et al*.,
435 2016).

436

437 **The correlations between photosynthesis and fluorescence over different spatial scales**

438 ChlF showed obvious seasonal variations with leaf spring development and autumn
439 senescence. Photosynthesis had similar seasonal patterns to ChlF parameters (Fig. 1) across the
440 season. Moreover, our results showed significant linear correlations between ChlF and
441 photosynthesis on different spatial scales (R^2=0.73 between F_s and $P_{apparent}$, 0.77 between
442 canopy-SIF and GPP_{EC}, 0.86 between GOME-2 SIF and MODIS-GPP for the entire growing
443 season) for this deciduous forest (Fig. 4c, 4d), which suggested that SIF may better capture the

seasonal change of GPP (carbon flux) in temperate deciduous forest ecosystems compared to existing models (e.g. GPP=APAR* ε) and satellite data products.

Simultaneously measured leaf-based ChlF and $P_{apparent}$ values are needed to link canopy SIF with GPP, with estimated $P_{apparent}/F_s$ as the leaf-level physiological basis of the model in place of the fixed ratio of GPP/SIF. The major assumptions of this model were (1) that both fluorescence and photosynthesis can be calculated as a product of absorbed radiance and light conversion efficiency across different spatial scales, and (2) that the mean value of ε_L from different canopy layers equals integrated canopy ε_C. It should be noted that the second assumption may slightly overestimate the low canopy's contributions to integrated canopy fluorescence and photosynthesis capacities, since the upper canopy should contribute more to the whole forest canopy though ε of upper canopy leaves may be limited by photoinhibition under high light condition (Niinemets and Kull, 2001). However, our leaf samples involved sunlit, shaded, sunlit-shaded foliage from different canopy layers. So the average of leaf scale ε should be close to the integrated ecosystem ε (Middleton *et al*., 2009). This model eliminated the estimation of APAR, which relates to leaf physiology and canopy structure, based on the assumption that the average value of ε_L from different canopy levels can represent the whole canopy ε_C. Estimating APAR from NDVI may lead to a relatively inaccurate GPP value due to noise and errors in measuring NDVI, especially from satellite products (Yuan *et al*., 2007). The significant relationship between GPP_{SIF} and GPP_{EC} (the slope of linear relationship between GPP_{SIF} and GPP_{EC} was close to 1 with the intercept as 0; Fig. 6) supports the feasibility of the model (Eq. 10), indicating that SIF may provide an additional approach to estimate the seasonality of photosynthesis for the deciduous forest. However, the points with high GPP_{SIF} value (GPP_{SIF}>25 μmol m^{-2} s^{-1}) were seriously deviated from the modeled line, which may be caused by the high

467 $P_{apparent}$ values measured on those two days (with relatively high air temperature and low
468 humidity). Therefore, we should be cautious about the maximum values of GPP_{SIF} and GPP_{EC}. In
469 addition, the significant linear relationships between leaf- level ChlF and $P_{apparent}$ when measured
470 under the same conditions, confirm the correlation between SIF and GPP values at larger scale
471 that were obtained from different monitoring sensors.

472 The correction coefficient, *c*, is important for the calculation of F_s which was assumed as
473 an instrument-specific constant representing the real meaning of leaf-scaled fluorescence values
474 measured by LI-6400 fluorometer. The uncertainties in *c* are due to $APAR_L$, $APAR_C$, canopy-SIF,
475 and leaf-F_s. Leaf-F_s was measured at a central wavelength of 710 nm (the range is between 700
476 and 715 nm), but canopy-SIF was measured at 760 nm wavelength including both PSI and PSII
477 fluorescence signals. Thus, PAM fluorescence included fluorescence information in the
478 wavelength that was not measured by canopy-SIF, and canopy SIF may be influenced by PSI
479 fluorescence that was very low (in contrast to PSII) and constant under light (Porcar-Castell *et al.*,
480 2014). It should also be mentioned that the radiometric unit of SIF is useful for scaling or
481 comparing to other ecosystems (e.g. Eq. 9), since SIF is based on spectral measurements of
482 radiometrically calibrated radiances (solar irradiance and vegetation radiance). In the future, it
483 would be useful to measure solar induced components of fluorescence to capture both downward
484 and upload signals form leaves (Wittenberghe *et al*. 2015).

485

486 **SIF and SIF-derived GPP correlate with chlorophyll content and other traits**

487 SIF and its derived GPP show a strong seasonal pattern that is affected by seasonal
488 variation in canopy chlorophyll content (Wittenberghe *et al*., 2013; Gitelson and Gamon, 2015).
489 In spring, leaf fluorescence and photosynthesis generally increase with the increasing chlorophyll

content after green-up; while in autumn, leaf fluorescence and the photosynthetic rate reduced associated with leaf physiological properties, especially in chlorophyll content, with declining with leaf aging and senescence (Fig. 7a) (David *et al*., 1998). Over the growing season, SIF-derived GPP show the significant correlations with vegetation greenness index (NDVI) and canopy structural parameter (LAI) (R^2=0.35 between GPP_{SIF} and LAI; R^2=0.36 between GPP_{SIF} and NDVI; $p<0.0001$) (Fig. 7b, 7c), which are widely used to monitor the seasonal changes of terrestrial ecosystems that represent the growing season length and carbon uptake period (Baret *et al*., 2007; Zarco-Tejada *et al*., 2013). Therefore, ChlF can be a powerful and sensitive tool to monitor the seasonal cycle of photosynthetic activity for deciduous vegetation (Campbell *et al*., 2008; Rohacek *et al*. 2008).

Furthermore, our SCOPE simulation stated the independent influence of leaf chlorophyll content and vegetation structure on SIF variability for unstressed C3 canopy. Fig. 8 revealed that the SIF_{760} remained increasing with LAI since more leaves emit more SIF_{760}, and the growth rate of SIF_{760} became slower under high LAI probably due to little light penetrated through the upper canopy and absorbed by lower canopy within a high-density canopy (Verrelst *et al*., 2015; Zhang *et al*., 2016). However, chlorophyll content (Cab) had more complex effects on SIF_{760}. At the initial stage of Cab development, SIF_{760} increased with Cab; whereas SIF_{760} became saturated at the high chlorophyll contents due to the saturation of light absorption by chlorophyll molecules at the high chlorophyll contents (Porcar-Castell *et al*., 2014). Zhang *et al*. (2016) have evaluated the SCOPE models with field measurements of SIF at Harvard Forest, and showed that the models were generally consistent with the field measurements.

In summary, our study links leaf-level fluorescence with canopy-level SIF, and reveals the correlations between fluorescence and photosynthesis over different spatial scales. The linear relationships between ChlF and photosynthesis during the growing season of canopy reflected that ChlF observations provide a powerful proxy to estimate global C budget. Moreover, sensitivity of ChlF signals provides a useful tool to understand the dynamic processes of vegetation growth in terrestrial ecosystems. We present a model to estimate GPP, with the goal of tracking seasonal variation of GPP using tower-based SIF data in conjunction with concurrently measured leaf steady-state ChlF and photosynthesis. The estimated GPP_{SIF} is comparable with the measured GPP_{EC}. The physiological information provided by the PAM fluorescence measurements at the leaf scale may provide a pathway to better understand and establish the relationship between ChlF, electron transport, and photosynthesis across leaves and canopies.

Acknowledgements

We would like to thank Harvard Forest for providing site and logistic support during our research. This research was supported by U.S. Department of Energy Office of Biological and Environmental Research Grant DE-SC0006951, National Science Foundation Grants DBI-959333 and AGS-1005663, and the University of Chicago and the MBL Lillie Research Innovation Award to J. Tang, National Science Foundation of China Grants (41671421) to Y. Zhang, and China Scholarship Council (CSC) to H. Yang.

References

Baker NR (2008) Chlorophyll fluorescence: a probe of photosynthesis in vivo. *Annual Review of Plant Biology*, **59**, 659-668.

534 Baret F, Hagolle O, Geiger B *et al*. (2007) LAI, fAPAR and fCover CYCLOPES global products
535 derived from VEGETATION. *Remote Sensing of Environment*, **110**, 275-286.
536 Bolhar-Nordenkampf HR, Long SP, Baker NR, Oquist G, Schreiber U, Lechner EG (1989)
537 Chlorophyll fluorescence as a probe of the photosynthetic competence of leaves in the
538 field: a review of current instrumentation. *Functional Ecology*, **3**, 497-514.
539 Bradbury M, Baker NR (1981) Analysis of the slow phases of the in vivo chlorophyll
540 fluorescence induction curve. Changes in the redox state of photosystem II electron
541 acceptors and fluorescence emission from photosystems I and II. *Biochimica Et*
542 *Biophysica Acta*, **635**, 542-551.
543 Campbell PKE, Middleton EM, Corp LA, Kim MS (2008) Contribution of chlorophyll
544 fluorescence to the apparent vegetation reflectance. *Science of The Total Environment*, **404**,
545 433-439.
546 Damm A, Elbers J, Erler A *et al*. (2010) Remote sensing of sun-induced fluorescence to improve
547 modeling of diurnal courses of gross primary production (GPP). *Global Change Biology*,
548 **16**, 171-186.
549 David MM, Coelho D, Barrote I, Correia MJ (1998) Leaf age effects on photosynthetic activity
550 and sugar accumulation in droughted and rewateredLupinus albus plants. *Australian*
551 *Journal of Plant Physiology,* **25**, 299-306.
552 Field CB, Randerson JT, Malmström CM (1995) Global net primary production: Combining
553 ecology and remote sensing. *Remote Sensing of Environment*, **51**, 74-88.
554 Flexas J, Escalona JM, Evain S, Gulıas J, Moya I, Osmond CB, Medrano H (2002) Steady-state
555 chlorophyll fluorescence (Fs) measurements as a tool to folloe variations of net CO_2

556 assimilation and stomatal conductance during water-stress in C_3 plants. *Physiologia*
557 *Plantarum*, **114**, 231-240.
558 Frankenberg C, Fisher JB, Worden J *et al*. (2011) New global observations of the terrestrial carbon
559 cycle from GOSAT: Patterns of plant fluorescence with gross primary productivity.
560 *Geophysical Research Letters*, **38**, 351-365.
561 Galle A, Florez-Sarasa I, Tomas M, Pou A, Medrano H, Ribas-Carbo M, Flexas J (2009) The role
562 of mesophyll conductance during water stress and recovery in tobacco (*Nicotiana*
563 *sylvestris*): acclimation or limitation?. *Journal of Experimental Botany*, **60**, 2379-2390.
564 Genty B, Briantais JM, Baker NR (1989) The relationship between the quantum yield of
565 photosynthetic electron transport and quenching of chlorophyll fluorescence. *Biochimica*
566 *Et Biophysica Acta*, **990**, 87-92.
567 Gitelson AA, Gamon JA (2015) The need for a common basis for defining light-use efficiency:
568 Implications for productivity estimation. *Remote Sensing of Environment*, **156**, 196-201.
569 Grace J, Nichol C, Disney M, Lewis P, Quaife T, Bowyer P (2007) Can we measure terrestrial
570 photosynthesis from space directly, using spectral reflectance and fluorescence?**.** *Global*
571 *Change Biology*, **13**, 1484-1497.
572 Guan K, Berry JA, Zhang Y, Joiner J. Guanter L, Badgley G, Lobell DB (2016) Improving the
573 monitoring of crop productivity using spaceborne solar-induced fluorescence. *Global*
574 *Change Biology*, **22**, 716-726.
575 Guanter L, Dudhia A, Lewis PE, Gómez-Dans J, Kuze A, Suto H, Grainger RG (2012) Retrieval
576 and global assessment of terrestrial chlorophyll fluorescence from GOSAT space
577 measurements. *Remote Sensing of Environment*, **121**, 236-251.

578 Guanter L, Rossini M, Colombo R, Meroni M, Frankenberg C, Lee JE, Joiner J (2013) Using field
579 spectroscopy to assess the potential of statistical approaches for the retrieval of
580 sun-induced chlorophyll fluorescence from ground and space. *Remote Sensing of*
581 *Environment*, **133**, 52-61.
582 Guanter L, Zhang Y, Jung M *et al*. (2014) Global and time-resolved monitoring of crop
583 photosynthesis with chlorophyll fluorescence. *Proceedings of the National Academy of*
584 *Sciences*, **111**, E1327-E1333.
585 Heinsch FA, Zhao M, Running SW *et al*. (2006) Evaluation of Remote Sensing Based Terrestrial
586 Productivity From MODIS Using Regional Tower Eddy Flux Network Observations.
587 *IEEE Transactions on Geoscience and Remote Sensing*, **44**, 1908-1925.
588 Joiner J, Yoshida Y, Vasilkov AP, Yoshida Y, Corp LA, Middleton EM (2011) First observations of
589 global and seasonal terrestrial chlorophyll fluorescence from space. *Biogeosciences*, **8**,
590 637-651.
591 Joiner J, Yoshida Y, Vasilkov AP *et al*. (2012) Filling-in of near-infrared solar lines by terrestrial
592 fluorescence and other geophysical effects: simulations and space-based observations from
593 SCIAMACHY and GOSAT. *Atmospheric Measurement Techniques*, **5**, 809-829.
594 Joiner J, Guanter L, Lindstrot R *et al*. (2013) Global monitoring of terrestrial chlorophyll
595 fluorescence from moderate-spectral-resolution near-infrared satellite measurements:
596 methodology, simulations, and application to GOME-2. *Atmospheric Measurement*
597 *Techniques*, **6**, 2803-2823.
598 Jung M, Reichstein M, Margolis HA *et al*. (2011) Global patterns of land- atmosphere fluxes of
599 carbon dioxide, latent heat, and sensible heat derived from eddy covariance, satellite, and
600 meteorological observations. *Journal of Geophysical Reasearch*, **116**, G00J07.

601 Kitajima M, Butler WL (1975) Quenching of chlorophyll fluorescence and primary
602 photochemistry in chloroplasts by dibromo-thymoquinone. *Biochimica Et Biophysica*
603 *Acta*, **76**, 105-115.
604 Larcher MW, Cernusca A (1985) Mikrocomputergesteuerte mobile Anlage zum
605 fluoro-metrischen Nachweis von Photosynthesestörungen. *Sitzungsber österr Akad Wiss*
606 *Math-Naturwiss K*, **194**, 45-64.
607 Lee JE, Frankenberg C, van der Tol C *et al*. (2013) Forest productivity and water stress in
608 Amazonia: Observations from GOSAT chlorophyll fluorescence. *Proceedings of the Royal*
609 *Society B: Biological Sciences*, **280**, 176-188.
610 Lee JE, Berry JA, Van der Tol C *et al*. (2015) Simulations of chlorophyll fluorescence
611 incorporated into the Community Land Model version 4. *Global Change Biology*, **21**,
612 3469-3477.
613 Long SP, Bernacchi CJ (2003) Gas exchange measurements, what can they tell us about the
614 underlying limitations to photosynthesis? Procedures and sources of error. *Journal of*
615 *Experimental Botany*, **54**, 2393-2401.
616 Maxwell K, Johnson GN (2000) Chlorophyll fluorescence—a practical guide. *Journal of*
617 *Experimental Botany*, **51**, 659-668.
618 Medlyn BE (1998) Physiological basis of the light use efficiency model. *Tree Physiology*, **18**,
619 167-176.
620 Meroni M, Rossini M, Guanter L, Alonso L, Rascher U, Colombo R, Moreno J (2009) Remote
621 sensing of solar-induced chlorophyll fluorescence: Review of methods and applications.
622 *Remote Sensing of Environment*, **113**, 2037-2051.

623 Middleton EM, Cheng YB, Hilker T, Black TA, Krishnan P, Coops NC, Huemmrich KF (2009)
624 Linking foliage spectral responses to canopy-level ecosystem photosynthetic light-use
625 efficiency at a Douglas-fir forest in Canada. *Canadian Journal of Remote Sensing*, **35**,
626 166-188.
627 Migliavacca M, Galvagno M, Cremonese E *et al*. (2011) Using digital repeat photography and
628 eddy covariance data to model grassland phenology and photosynthetic CO2 uptake.
629 *Agriculture and Forest Meteorology,* **151**, 1325-1337.
630 Miura T, Huete AR, Yoshioka H (2000) Evaluation of sensor calibration uncertainties on
631 vegetation indices for MODIS. *IEEE Transactions on Geoscience and Remote Sensing*, **38**,
632 1399-1409.
633 Monteith JL (1972) Solar Radiation and Productivity in Tropical Ecosystems. *The Journal of*
634 *Applied Ecology*, **9**, 747-766.
635 Monteith JL (1977) Climate and the efficiency of crop production in Britain. *Philosophical*
636 *Transactions of the Royal Society of London*, **281**, 277-294.
637 Naumann JC, Young DR, Anderson JE (2007) Linking leaf chlorophyll fluorescence properties
638 to physiological responses for detection of salt and drought stress in coastal plant species.
639 *Physiologia Plantarum*, **131**, 422-433.
640 Niinemets Ü, Kull O (2001) Sensitivity of photosynthetic electron transport to photoinhibition in
641 a temperate deciduous forest canopy: Photosystem II center openness, non-radiative
642 energy dissipation and excess irradiance under field conditions. *Tree Physiology*, **21**,
643 899-914.
644 Prince SD, Goward SN (1995) Global primary production: A remote sensing approach. *Journal of*
645 *Biogeography*, **22**, 815-835.

Porcar-Castell A, Tyystjärvi E, Atherton J *et al*. (2014) Linking chlorophyll a fluorescence to photosynthesis for remote sensing applications: mechanisms and challenges. *Journal of Experimental Botany*, **65**, 4065-4095.

Rascher U, Liebig M, Luttge U (2000) Evaluation of intant light-response curves of chlorophyll fluorescence parameters obtained with a portable chlorophyll fluorometer on site in the field. *Plant Cell and Environment*, **23**, 1397-1405.

Rascher U, Agati G, Alonso L *et al*. (2009) CEFLES2: the remote sensing component to quantify photosynthetic efficiency from the leaf to the region by measuring sun-induced fluorescence in the oxygen absorption bands. *Biogeosciences Discuss*, **6**, 2217-2266.

Reichstein M, Falge E, Baldocchi D *et al*. (2005) On the separation of net ecosystem exchange into assimilation and ecosystem respiration: Review and improved algorithm, *Global Change Biology*, **11**, 1424-1439.

Rohacek K, Soukupova J, Bartak M (2008) Chlorophyll fluorescence: A wonderful tool to study plant physiology and plant stress. *Plant Cell Compartments – Selected Topics*, 41-104.

Rossini M, Meroni M, Migliavacca M *et al*. (2010) High resolution field spectroscopy measurements for estimating gross ecosystem production in a rice field. *Agricultural and Forest Meteorology*, **150**, 1283-1296.

Seaton GGR, Walker DA (1990) Chlorophyll fluorescence as a measure of photosynthetic carbon assimilation. *Proceedings of the Royal Society of London*, **242**, 29-35.

Turner DP, Ritts WD, Cohen WB *et al*. (2003) Scaling gross primary production (GPP) over boreal and deciduous forest landscapes in support of MODIS GPP product validation. *Remote Sensing of Environment*, **88**, 256-270.

668 Van der Tol C, Verhoef W, Rosema A (2009a) A model for chlorophyll fluorescence and
669 photosynthesis at leaf scale. *Agricultural and Forest Meteorology*, **149**, 96-105.
670 Van der Tol C, Verhoef W, Timmermans J, Verhoef A, Su Z *et al*. (2009b) An integrated model of
671 soil-canopy spectral radiance observations, photosynthesis, fluorescence, temperature and
672 energy balance. *Biogeosciences Discussions*, **6**, 6025–6075.
673 Van der Tol C, Berry JA, Campbell PKE, Rascher U (2014) Models of fluorescence and
674 photosynthesis for interpreting measurements of solar-induced chlorophyll fluorescence.
675 *Journal of Geophysical Research: Biogeosciences*. **119**, 2312-2327.
676 Verrelst J, Rivera PR, Van der Tol C *et al*. (2015) Global sensitivity analysis of the SCOPE model:
677 What drives simulated canopy-leaving sun-induced fluorescence? *Remote Sensing of*
678 *Environment*, **166**, 8–21.
679 Williams M, Richardson AD, Reichstein M *et al*. (2009) Improving land surface models with
680 FLUXNET data. *Biogeosciences*, **6**, 1341-1359.
681 Wittenberghe SV, Alonso L, Verrelst J *et al*. (2013) Upward and downward solar-induced
682 chlorophyll fluorescence yield indices of four tree species as indicators of traffic pollution
683 in Valencia. *Environmental Pollution*, **173**, 29-37.
684 Wittenberghe SV, Alonso L, Verrelst J, Moreno J, Samson R (2015) Bidirectional sun-induced
685 chlorophyll fluorescence emission is influenced by leaf structure and light scattering
686 properties-A bottom-up approach. *Remote Sensing of Environment*, **158**, 169-179.
687 Wohlfahrt G, Gu L (2015) The many meanings of gross photosynthesis and their implication for
688 photosynthesis research from leaf to globe. *Plant, Cell and Environment*, **38**, 2500–2507.

689 Xu ZZ, Zhou GS, Wang YL, Han GX, Li YJ (2008) Changes in chlorophyll Fluorescence in
690 Maize Plants with Imposed Rapid Dehydration at Different Leaf Ages. *Journal of Plant*
691 *Growth Regulation*, **27**, 83-92.
692 Yang X, Tang J, Mustard JF *et al*. (2015) Solar-induced chlorophyll fluorescence that correlates
693 with canopy photosynthesis on diurnal and seasonal scales in a temperate deciduous forest.
694 *Geophysical Research Letters*, **42**, 2977-2987.
695 Yang X, Tang J, Mustard JF *et al*. (2016) Seasonal variability of multiple leaf traits captured by
696 leaf spectroscopy at two temperate deciduous forests. *Remote Sensing of Environment*,
697 **179**, 1-12.
698 Yang H, Tang J, Heskel M, Yang X, Sun S (2016) Seasonal variations of leaf and canopy
699 properties tracked by ground-based NDVI imagery in a temperate forest. **In review.**
700 Yuan W, Liu S, Zhou G *et al*. (2007) Deriving a light use efficiency model from eddy covariance
701 flux data for predicting daily gross primary production across biomes. *Agricultural and*
702 *Forest Meteorology*, **143**, 189-207.
703 Zarco-Tejada PJ, Catalina A, González MR, Martín P (2013) Relationships between net
704 photosynthesis and steady-state chlorophyll fluorescence retrieved from airborne
705 hyperspectral imagery. *Remote Sensing of Environment*, **136**, 247-258.
706 Zhao M, Running SW (2010) Drought-Induced Reduction in Global Terrestrial Net Primary
707 Production from 2000 Through 2009. *Science*, **329**, 940-943.
708 Zhang Y, Guanter L, Berry JA *et al*. (2014) Estimation of vegetation photosynthetic capacity from
709 space-based measurements of chlorophyll fluorescence for terrestrial biosphere models.
710 *Global Change Biology*, **20**, 3727-3742.

711 Zhang Y, Guanter L, Berry JA *et al*. (2016) Model-based analysis of the relationship between
712 sun-induced chlorophyll fluorescence and gross primary production for remote sensing
713 applications. *Remote Sensing of Environment*, **187**, 145-155..
714
715